Anisotropic Gradient-based Filtering for Object Segmentation in Medical Images

Ana João[+], Alberto Gambaruto[*], Adélia Sequeira[+]

[+] *Departamento de Matemática and Centro de Matemática Computacional e Estocástica (CEMAT)/IST*
Instituto Superior Técnico, University of Lisbon
Av. Rovisco Pais 1, 1049-001 Lisboa, Portugal.

[*] *Department of Mechanical Engineering*
University of Bristol
Queen's Building, University Walk, Bristol BS8 1TR, UK.

Abstract

A four-step approach for image filtering and object segmentation is explored. The key steps are: i) a low-pass digital differentiator is used to compute the image gradient (vector) field; ii) the regularised anisotropic diffusion method is used to filter this vector field; iii) the modified image is reconstructed from the filtered gradient field as a least-squares best fit; iv) object segmentation is performed on the reconstructed image. The advantages of this approach is the easier identification of noise in the gradient field, and consequently the image filtering can be more effective. The least-squares fit allows for non-local adjustment to the image to improve overall smoothness while enhancing object contrast. Importantly one can also ensure that relevant feature boundary locations are preserved, while appearing smoother due to the filtering. The proposed filtering methodology is compared to image filtering applied directly to the image intensity. A set of challenging medical images of mammography exams and confocal microscopy experiments are used as numerical tests.

Keywords:
non-linear anisotropic filtering, fractional derivatives, object segmentation, regularised backward and forward anisotropic diffusion (RBAF), image reconstruction from gradient field

1. Introduction

Image filtering to remove or reduce the presence of noise, is frequently employed to improve the visual quality of an image and is often a component of an image processing task or pipeline. Medical image processing is additionally concerned with the accuracy of feature identification and segmentation. Consequently, image filtering techniques are extensively used in many rendering and image processing pipelines, prior to analysis of image content.

Medical images are prone to corruption by noise, imaging artifacts, poor contrast and limited resolution. Noise can be either correlated or uncorrelated, depending on the image

acquisition modality used. Regardless of the image characteristics, noise acts as the localised undesirable change (pixel-wise or a clustered neighbourhood of pixels) in the image intensity. Therefore, these are associated to non-smooth intensity variations which locally result in higher gradients and increased variance of the image intensity.

In the present work, the purpose of the filtering is to achieve higher accuracy in feature identification and segmentation, with application to the medical imaging and derived research communities. As test cases for numerical evaluation of the novel proposed filtering approach, we look at mammogram datasets and experimental micro-haemodynamics, from which we respectively wish to segment automatically any lesions/abnormalities or flowing red blood cells. Therefore, for the filtering process to be successful, it should neither deteriorate nor distort the image features, namely object boundaries. From a medical or clinical point of view, in order to be effective, the image processing should allow for improved clinical evaluation and faster or more satisfactory diagnosis.

Despite the broad range of algorithms developed for image filtering, most methods work by altering the image intensity scalar field directly. Some well known methods for image denoising include: median filter [24], anisotropic diffusion and its regularisations [42, 13, 15, 3, 14], total variation diminishing [43], Wiener filter [52, 26], fuzzy-image filters [48], and many more. Various studies with analysis of different method and applications to medical images can be found in [29, 35, 28, 40]. However, a smaller number of works have shown promising results when the image gradient field is processed directly. Non-homogeneous isotropic diffusion was applied to the image gradient in [50] as a preliminary investigation, showing promising results by visual inspection. In [6] high dynamic range images were obtained by attenuating the magnitudes of large gradients of the luminance image. A topographic primal sketch of the image gradient was used adopted in [11] to reduce noise, improve contrast enhancement, thin object contours and preserve feature edges, for a test set of medical images.

Here we adopt the approach of filtering the image by acting on the image intensity gradient (vector) field. Processing the image gradient field has a number of advantages, including: i) easier noise identification, such that any filtering method can be more effective; ii) easier identification of feature boundaries or contrasts, such that they are preserved as well as enhanced or restored; iii) local correction to the gradient field results in non-local image adjustment, allowing for a simple means to improve the dynamic range and object contrast. Having modified the gradient field, we recover the modified image through a global least-squares best fit approach [21, 11], which additionally acts as a smoothing operation.

We bring together a set of image processing tools and the proposed technique is quite effective, is conceptually simple, robust and automatic. Specifically, we adopt the regularised backward and forward anisotropic diffusion (RBAF) method for filtering [16, 18], based on fractional derivatives which are interpreted by means of a Fourier expansion. An automatic means of setting the diffusion coefficient and integration time for the diffusion equation was adopted, involving a segregated exhaustive search to ensure reproducibility [27]. The focus of proposed technique is the segmentation of objects in medical images containing noise, artefacts and of limited resolution, but otherwise have evident feature boundaries.

Evaluation of the proposed method is performed using test medical images, comparing results of segmentation when filtering is applied to the image intensity versus the image intensity gradient field.

The outline of the paper is as follows. Section 2 presents the novel proposed four-step method, detailing the key stages in detail. Section 3 outlines the key results, based on numerical tests on several images pertaining to clinical mammography scans and confocal microscopy images of experimental micro-haemodynamics. The findings are discussed further in Section 4 and finally conclusions are drawn in Section 5.

2. Methods

The filtering of images is commonly performed directly on the pixel intensities, a grey-scale scalar field in the case of most medical images, with few works instead applying the filtering to the image gradient field. Two crucial advantages for filtering in the gradient domain are, firstly, the possibility to directly control some biases of the human visual system, since gradients are integral to how we perceive images. Studies show that our visual system has difficulties identifying image intensities, but instead perceives local contrast and hence image gradients [7, 34, 2]. Secondly, gradient-based methods can modify high-level image features, such the object shape and contrast in a much simpler way. Local adjustments to image gradients can produce global changes in an image [8, 11], which is not the case if working with the image intensity directly.

The overall approach proposed here, can be summarised in the following four-step process:

Step 1. compute the gradient vector field of the image intensity scalar field, with a finite difference scheme of predetermined accuracy and pass-band (see Section 2.1);

Step 2. process the gradients using the *Regularised Backward and Forward Anisotropic Diffusion* (RBAF) as the filtering method, with optimal parameters computed according to [27] (see Section 2.2);

Step 3. reconstruct the image from the filtered gradient field using a least-squares minimisation, satisfying the Euler-Lagrange equation, which reduces to solving a 2D Poisson problem (see Section 2.3);

Step 4. extract the desired features, using either the *marker-based watershed* method or the *zero-crossing of the second directional derivatives* (see Section 2.4).

For comparison purposes, we substitute steps 1-3 of the process with a single step in which the filtering is applied directly to the image intensities, as is the case in more classical approaches to image processing. The RBAF method is again used for the filtering, and the final stage involving image segmentation then follows. This alternative approach, for comparison purposes, is hence a two-step process:

Step 1. filter the image pixel intensities, using the *Regularised Backward and Forward Anisotropic Diffusion* (RBAF), with optimal parameters computed according to [27];

Step 2. extract the desired features, using either the *marker-based watershed* method or the *zero-crossing of the second directional derivatives*.

2.1. Finite difference operator for computing the gradient

Computing the gradient field of an image (Step 1) is not straightforward, especially when images have limited resolution and are corrupted by noise. Some basic approaches to alleviate this problem include use of the Sobel operator or convolution with a Gaussian function, while more detailed discussion on the topic can be found in [5, 53, 1, 38, 51]. For simplicity, the centred second-order accurate finite difference scheme is used, which is known to act as a low-pass digital differentiator [9, 30]. While use of more sophisticated discrete differentiation schemes may improve the quality of the proposed method of filtering, by employing the centred finite difference scheme we can highlight the robustness and effectiveness of the proposed four-step filtering process.

2.2. Regularised backward and forward anisotropic diffusion (RBAF) method

Filtering methods based on partial differential equations (PDE) have been widely used in image processing due to their ability to reduce noise while preserving important structures. A popular method, known as the Perona-Malik (PM) method [42], makes use of a non-linear anisotropic diffusion PDE, in which the diffusion coefficient of image intensities depends on the gradient magnitude:

$$\frac{\partial I}{\partial t} = \mathrm{div}(\mathrm{c}\nabla \mathrm{I}), \tag{1}$$

with the spatially varying diffusion coefficient, a scalar, given by

$$c = \frac{1}{1 + \left(|\nabla I|/\beta\right)^2}. \tag{2}$$

where the constant β normalises the image gradient intensity based on the objects and noise present in the image [42, 27]. Since boundaries of objects within an image are identifiable as locally higher gradients of the pixel intensity, by making the diffusion coefficient a function of $|\nabla I|$ one can ensure that smoothing occurs *within* a region rather than *across* region boundaries. As seen from Eq. 2, the diffusion coefficient is in fact chosen to be a decreasing function of the image gradient magnitude. Alternative equations for the diffusion coefficient have been proposed in [42, 13, 15, 3, 19, 14] and in effect share the same underlying motivation and working principles though results may vary.

In [16, 18] and references therein, a set of different methods based on the anisotropic diffusion equation (Eq. 1) are reviewed. The model given by Eqs. 1-2 is known to be ill-posed, and in the present work we adopt one of the two regularised models proposed by [18] known as *Regularised Backward and Forward Anisotropic Diffusion* (RBAF) which offers a well-posed solution through use of fractional derivatives, achieving robust results [16, 19]. The diffusion coefficient, c takes the following form:

$$c(x, y, t) = \left(\frac{1}{1 + \left(|\nabla^{1-\epsilon} I|/\beta\right)^2} \right) \tag{3}$$

where $(1-\epsilon)$ is the order of the fractional derivative, and hence ϵ is the offset from the integer-order derivative. The local well-posedness of Eq. 3 is studied at length in [17], where it is shown to admit characteristic functions of smooth sets as stationary solutions. This is due to the reduction in non-linearity intensity obtained when $\epsilon > 0$. Furthermore, the fractional derivative used to compute the gradient results in a function with an integrable singularity along the boundary of the image, which is otherwise smooth [17]. Therefore the non-linearity applied to it gives at least a continuous function which vanishes exactly on the boundary. A fast Fourier transform (FFT) based pseudo-spectral discretisation is employed, leading to a simple means to attain fast and accurate computation of the fractional derivatives, though other approaches are possible [33].

In our four-step process, having computed the image gradient $\nabla I = [I_x, I_y]$ using a finite difference scheme (Step 1), each component of the gradient is then filtered using RBAF (Step 2). The two parameters required to perform the filtering are the coefficient β (see Eq. 3) and the total integration time T of the diffusion process (see Eq. 1). While these may be set *a priori*, an automatic and robust approach detailed in [27] is opted for instead, allowing for a tuned filtering algorithm that is independent of any user choices. In practice, the method detailed in [27] involves a two-step exhaustive search to identify parameter choices for β and T, based on rates-of-change of image quality metrics as the anisotropic diffusion filtering process evolves.

2.3. Gradient-based image filtering and restoration

Given a filtered gradient field, $(\nabla I)_{filtered} = G = [G_x, G_y]$, the goal is to reconstruct an image J such that ∇J is *as close as possible* to G. Since the original image gradient field has been modified, there is no guarantee that the *zero-curl* property ($\nabla \times G = 0$) holds, hence $\frac{\partial G_y}{\partial x} \neq \frac{\partial G_x}{\partial y}$. The consequence of not satisfying the zero-curl condition is that the path integral on G along any contour around a point will give a non-zero value, and hence the reconstructed surface J will depend on the integration path.

A similar problem is commonly known from *shape-from-shading*, where a depth field is reconstructed from images [55, 50, 21, 39, 22]. A survey of several methods is presented in [22], highlighting possible drawbacks of each approach. In [21, 22] a very efficient approach based on the Sylvester equations is proposed, though due to the symmetric finite difference scheme used, it is subject to a checkerboard effect [11]. An alternative approach based on mixed-order finite difference approximations was successfully adopted in [11], however this involves solving for a large overdetermined system of equations which is computationally expensive if methods such as singular value decomposition are adopted.

In the present work we look for a possible image J whose gradients are close to G in a least-squares sense. Hence, we wish to minimise the cost function given by:

$$r = \int \int \|\nabla J - G\|^2 \, \mathrm{dx} \, \mathrm{dy} \tag{4}$$

In order to minimise the cost function, the integrand must satisfy the Euler-Lagrange equation and the problem reduces to solving the Poisson equation [21, 23]:

$$\nabla^2 J = \nabla \cdot G \tag{5}$$

In this work the Poisson equation is solved by the discrete sine transform (DST) [10, 46, 12] and the Laplacian is approximated numerically by a second order centered-difference scheme.

2.4. Quality analysis

To compare the efficacy of the filtering methodologies and the quality of processed image, we focus on the segmentation accuracy for specific objects of interest in the datasets. Additionally, we make use of the mean square error (MSE), defined as:

$$MSE = \frac{1}{n \times m} \sum_{i=1}^{n} \sum_{j=1}^{m} [I_0(i,j) - I_T(i,j)]^2 \tag{6}$$

where I_0 and I_T are the original and filtered images, respectively, and $n \times m$ is the size of the image. We report the MSE as a measure of how much the images have changed compared to the original, providing insight into the precesses involved.

The segmentation methods used are *watershed transform* [44, 25, 45, 41] and *zero-crossing of the second directional derivatives* [36, 11, 20]. Here we employ the watershed transform method for the segmentation of lesions or abnormalities present in mammograms, following the promising results reported in [54, 32]. On the other hand, the method of identifying the locations of the zero-crossing of the second directional derivatives is employed here to segment red blood cells flowing in experimental micro-channels. This latter method has several benefits, including the reduction of perceived blurring that may occur when objects are out of focus [11, 20].

In the watershed transform [4], grey-level images are considered as topographic reliefs, and the method works by flooding the domain from its topographic minima. When two water fronts merge, a dam is created at the interface, and as the process continues closed contours may be identified. This method requires low computation time in comparison with other segmentation methods. To overcome the over-segmentation of the image, the marker-based watershed transformation detailed in [45] is employed.

In order to identify the locations of zero-crossing of the second directional derivatives, the first task is to compute, at each pixel, the spatial derivatives of the image intensity up to second order. The gradient vector (∇I) and the Hessian tensor ($\mathcal{H}$) can then be assembled. The locations of zero-crossing of the second directional derivatives must then satisfy

$$\tilde{\mathbf{n}}^T \mathcal{H} \tilde{\mathbf{n}} = 0, \qquad \text{with} \qquad \tilde{\mathbf{n}} = \frac{\nabla I}{|\nabla I|}, \tag{7}$$

where $\tilde{n}$ represents the unit normal vector to the isophote (contour of equal luminance).

3. Results

The effectiveness of the proposed four-step image processing methodology is evaluated by means of numerical tests on a set of medical images, chosen to be challenging test cases. The selected images belong to two dataset types: from clinically acquired mammogram exams,

Mammography images			**Confocal microscopy images**		
	Minimum Marker	*Maximum Marker*		*Mask size*	*Taylor expansion order*
Mammogram 1	9	20	**RBCs 1**	9	3
Mammogram 2	12	20	**RBCs 2**	5	3
Mammogram 3	5	20			
Mammogram 4	14	25			
Mammogram 5	15	22			
Mammogram 6	6	20			

Table 1: Parameter used for contour segmentation. For mammography images *marker-based watershed* method was used, while for the confocal microscopy images of red blood cells (RBCs) the *zero-crossing of the second directional derivatives* method were used.

and from confocal microscopy images of blood flow experiments in micro-channels. The difficulty in the mammogram images are: the loss of visibility of lesion/mass borders against the fatty background tissue, and the complex shape that the diseased tissue may take. In the red blood cell experiments the challenges are: the high level of noise, motion blur, instances when cells may be out of focus when lying off the focal plane, and the touching of adjoining cells or to the channel walls. Both datasets contain noise and have limited resolution. The experimental data of red blood cells flowing in micro-channels is obtained from high-speed confocal microscopy [31]. Mammography images are obtained from a dataset repository [47], for which regions of lesion are identified by the magenta square in Fig. 1a and the details of image test cases are as follows:

- *Mammogram 1*, (dataset ID = 152): Fatty background tissue; Architectural distortion; Benign.
- *Mammogram 2*, (dataset ID = 155): Fatty background tissue; Architectural distortion; Malign.
- *Mammogram 3*, (dataset ID = 181): Fatty glandular tissue; Speculated masses; Malign.
- *Mammogram 4*, (dataset ID = 209): Fatty glandular tissue; Calcification; Malign.
- *Mammogram 5*, (dataset ID = 226): Dense glandular tissue; Calcification; Benign.
- *Mammogram 6*, (dataset ID = 240): Dense glandular tissue; Calcification; Malign.

For simplicity in presenting and discussing the results, the notation adopted is as follows:

→ I denotes the original, unprocessed image;

→ I^F denotes the image obtained by filtering directly the image intensities (result of the two-step process);

→ J denotes the image obtained by reconstructing the filtered image gradient field (result of the four-step process).

To ensure repeatability of the results obtained and a meaningful comparison, the processing steps are largely automatic to avoid user chosen parameters that could affect repeatability. Those parameters which are user defined are those which control the segmentation process only, namely the minimum and maximum markers in the watershed method, and

the mask size and the monomial order (truncation of the Taylor expansion) for computing the zero-crossing of the second directional derivatives. The choice of these parameters is reported for completeness in Table 1. Additionally the fractional derivative value is set to $\epsilon = 0.1$, following the favorable results reported in [16, 14]

3.1. Analysis of the mammography dataset segmentation

Let us start by considering the six mammography images, chosen to cover different pathologies and breast abnormalities. The results of the image processing are presented and compared in Fig. 1. We observe that in most cases, the results for I^F indicate that the filtering process using the RBAF method with automatic parameter selection, applied directly to the image intensity, has successfully avoided blurring the important features, such as the breast contour and abnormality boundaries. The dataset 'mammogram 3' however shows a degree of whitening, with consequently poor segmentation results.

The level and presence of noise has been reduced to a greater extent for the results of J, for which the segmentation also provides consistently superior results in identifying the lesion/mass tissue of interest. We note that the segmentation of image J produces fewer individual regions, compared to results for images I or I^F, being robust to noise removal while retaining relevant object definition. Furthermore, the regions identified in the segmentation of J are consistent with the clinical evaluation and lesion localisation detailed in [47].

3.2. Analysis of the confocal microscopy dataset segmentation

Two images from experimental work involving of red blood cells (RBCs) flowing in microchannels have also been considered. In both images, the RBCs are seen to be in contact, of deformed shape, and slightly out of focus. In image 'RBCs 1' the cells are seen to be quasi circular in shape, while in image 'RBCs 2' the cells are elongated as they pass through the stenosis. The results of the image processing are presented and compared in Figs. 2-3.

Results of the confocal microscopy show that the RBAF method applied directly to the image intensity provides good noise reduction, however not as effective as when applied to the gradient field. This result is independent of the parameters β and T selected. We observe that the edge segmentation for image J are less prone to noise artefacts while maintaining accurate localisation. We have verified that continuing the diffusion process on I^F could further remove noise but it would also degrade the image by blurring features, hence degrading object boundary definitions.

In order to obtain a better appreciation of the results, we plot the image intensity and the intensity gradient over a line section of the images, as shown in Fig. 3. We observe that image I^F closely follows the original image I, and as expected the smaller features are attenuated while dominant edges (which are associated to the object edges) are preserved. We note from these line sections that image J deviates markedly from the original image I, though this does not seem apparent from visual inspection of the images. The reason for this is the effective noise removal when filtering is performed in the gradient field, as well as from the solution of the Possion equation to reconstruct image J by minimising Eq. 4. We also observe a small (within one pixel) distortion of the peaks in intensity gradient in J as

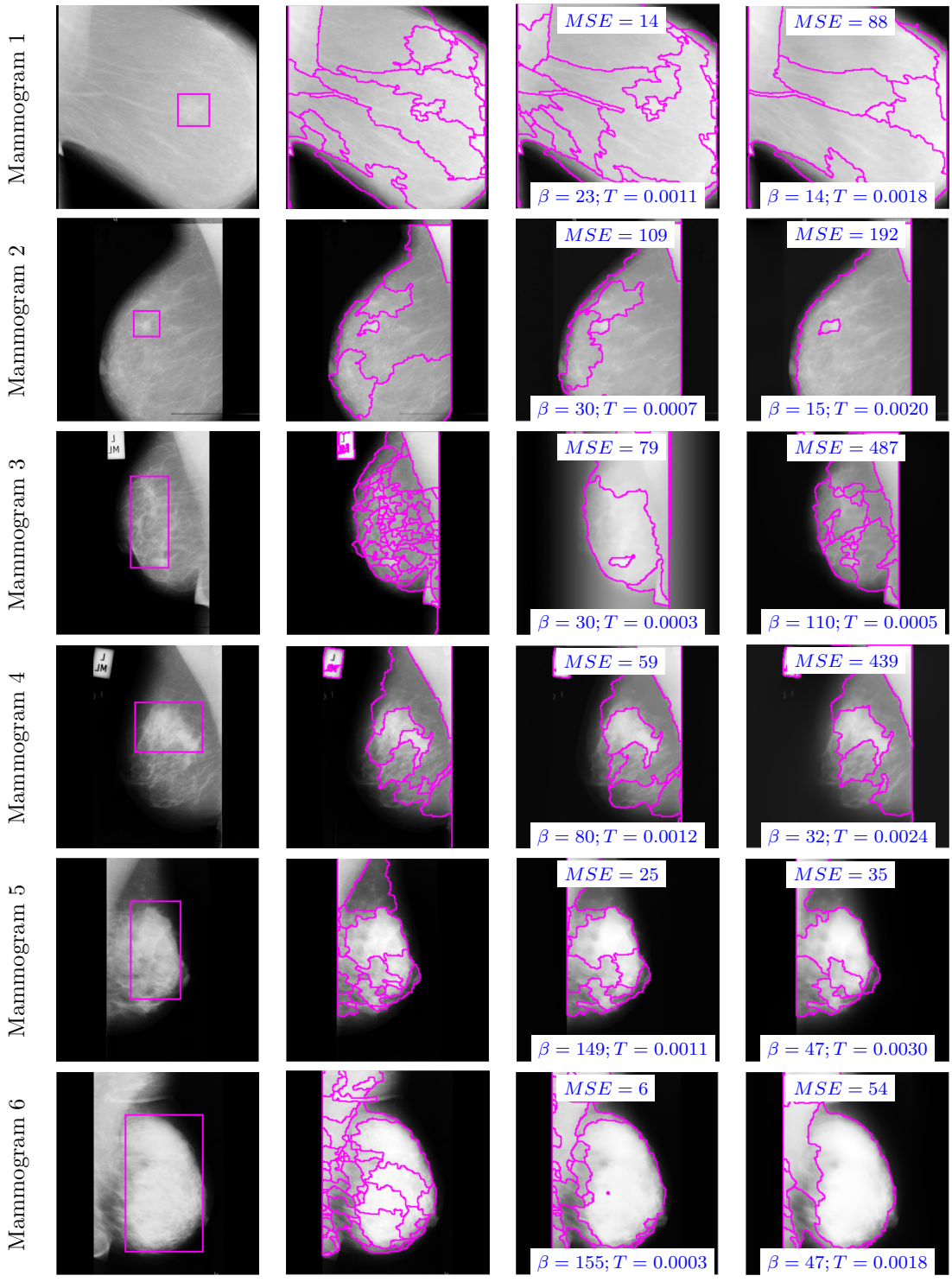

Figure 1: Mammography image dataset, with the (a) regions of interest (ROI) drawn on the original image, which indicate location of lesions. Result of the automatic watershed segmentation method for: (b) unprocessed original image; (c) image obtained by filtering the image intensities; (d) image obtained by filtering the image gradients and then reconstructing with the Poisson solver. The parameters used in the RBAF filtering are given below each image. The MSE values are given at the top of each image.

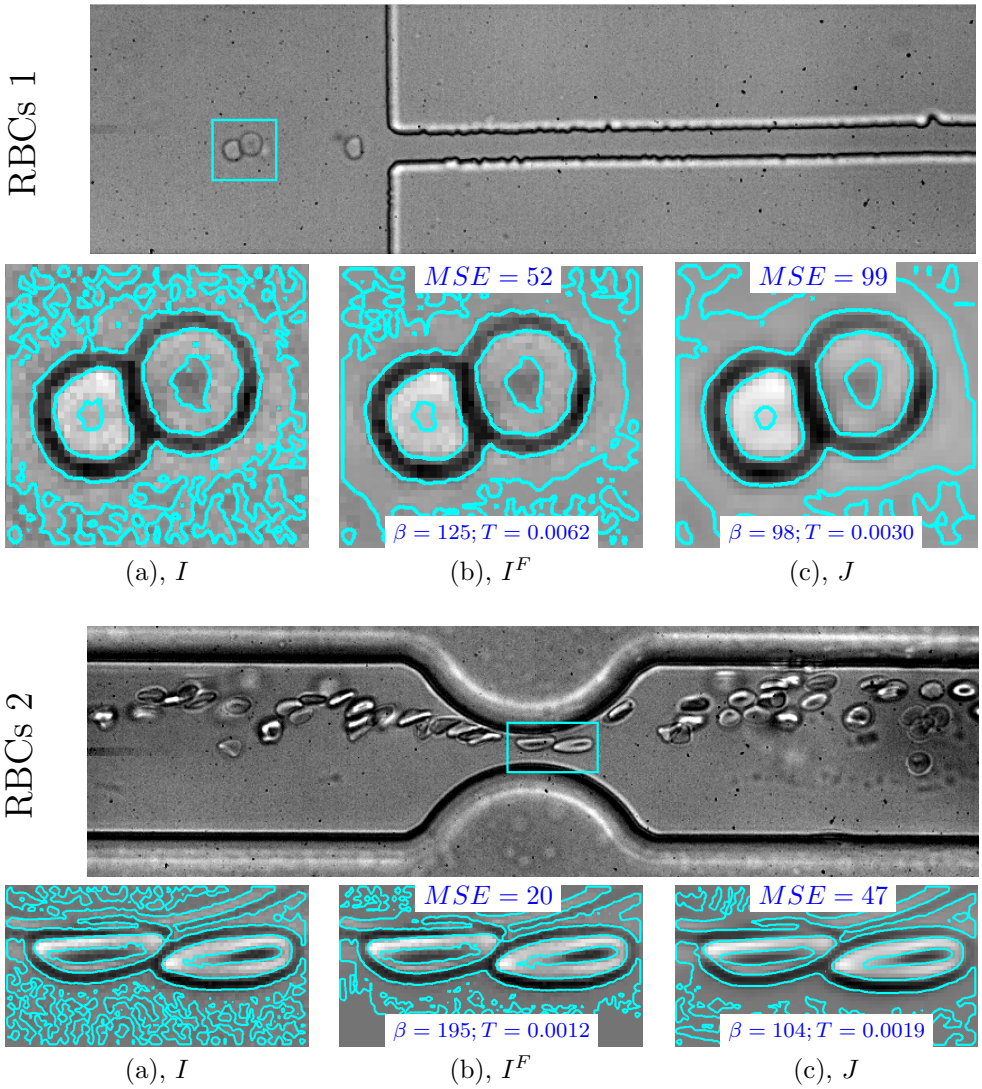

Figure 2: Confocal microscopy datasets (top: RBCs1, bottom: RBCs 2), with region of interest (ROI) drawn on the original image, and detail of the red blood cells identified. Result of the automatic *zero-crossing of the second directional derivative* segmentation method for: (a) unprocessed original image; (b) image obtained by filtering the image intensities; (c) image obtained by filtering the image gradients and then reconstructing with the Poisson solver. The parameters used in the RBAF filtering are given below each image. The MSE values are given at the top of each image.

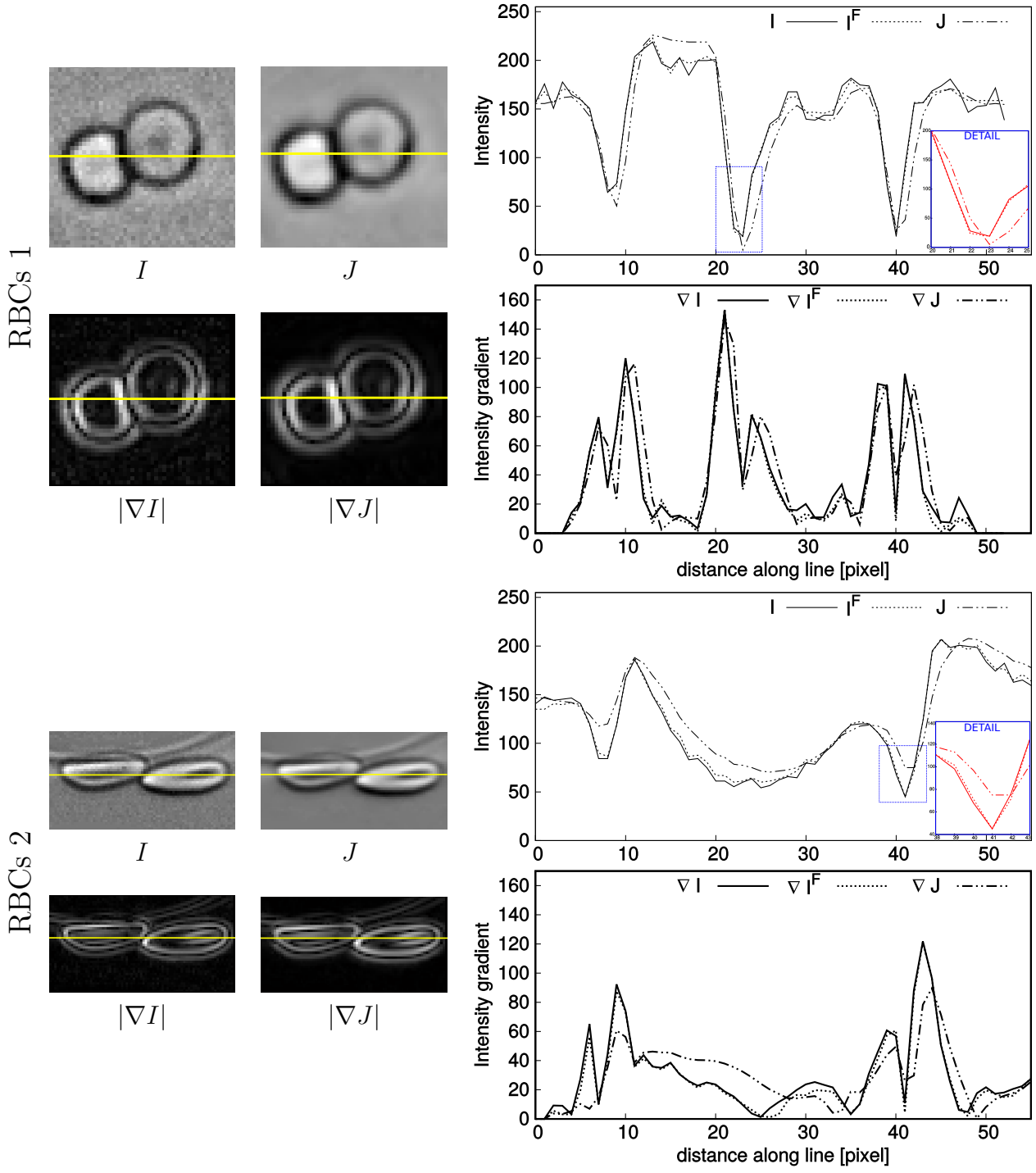

Figure 3: Confocal microscopy datasets (top: RBCs1, bottom: RBCs 2). Variation of image intensity and intensity gradient for images I, I^F and J, are plotted (on the right) along the yellow line section (shown in the set of images on the left).

compared to I, which is due to the higher order filtering which occurs when applying Eq. 3 to the image gradient field.

3.3. Analysis of the mean square error of the datasets

The MSE results, which compare the original image I to the processed images I^F and J, are reported above each image in Figs. 1-2. We observe a greater MSE for image J than for image I^F; the reason being that global changes occur in image J unlike the localised filtering observed in I^F. These global changes are due to the solution to the Poisson equation to reconstruct J, and can be visually appreciated in the line sections shown in Fig. 3.

4. Discussion

Images from clinical mammography exams and from experimental confocal microscopy micro-haemodynamics, have been used to test numerically the effects of filtering an image gradient field as opposed to the image intensity directly. The tools employed have previously separately been successfully applied to image processing, and we combine them into the proposed four-step scheme. Evaluation of the processing is specifically focused on object segmentation.

The filtered image and segmentation results obtained from the proposed four-step method are encouraging and overall superior to the standard two-step method. Results of the mammograms show correct delineation of lesion tissue while reducing effects of over segmentation. Results of the confocal microscopy images indicate smooth edge detection of the red blood cells, with accurate localisation and effective reduction of the background noise. Neighbouring objects are not merged during the segmentation and there is a reduced presence of spurious object identification.

The four-step method proposed has a number of desirable features in filtering and segmenting the dominant objects in medical images, as seen from the numerical tests. It is worth discussing these features in greater detail, providing an overarching motivation in support for the four-step method proposed. Firstly, we note that applying the aniosotropic diffusion (Eq. 1) with regularised diffusion coefficient as function of the image gradient magnitude (Eq. 3) on the image gradient field, can be understood as a higher order filter applied to the image. Since the diffusion coefficient is a function of the image gradient magnitude, and the filtering is applied to the image gradient field, in essence it appears as a function of second order derivatives of the image. Consequently, given that the RBAF method acts by smoothing within a region rather than across region boundaries, and we are acting on the image gradient field, we can expect object boundary localisation to be given by second order derivatives, in the spirit of the Marr-Hildreth edge detector [36]. Higher order anisotropic filtering methods, such as [13, 3, 19], also employ this physical reasoning. As such, since the object edge appear as a narrow band of high image gradient magnitude, by applying the RBAF filtering to this image gradient field we allow the smoothing to occur within this narrow band and not across it, maintaining good edge localisation. This promotes smoothing object contours when corrupted by noise, evident from inspection of Fig. 2, and providing a more uniform image gradient at object edges which results in clearer object segmentation

and fewer spurious edges being identified, as seen in Figs. 1-2. However, since the diffusion coefficient is in practice analogous to the higher order derivatives, strict edge localisation is not guaranteed. In fact we note from the line sections shown in Fig. 3 that the peak gradient magnitudes for image J do not align precisely with those of the original image I, while those of I^F do indeed align more accurately. The distortion is however below pixel resolution, and we can expect this to be true for any image with evident intensity discontinuity between object and background.

The reconstruction of the image from the filtered gradient field, by means of least-squares approach which leads to solving the Poisson equation, also plays an important role in the success of the four-step method. Noise present in the image is easily identifiable in the image gradient field, and effectively filtered by anisotropic diffusion, while dominant feature edges are preserved and will act as the primal sketch of the image [11]. Reconstructing the image by a least-squares fit will therefore be guided by this primal sketch of prevalent edges, further diminishing the presence of noise and small features in the image. We see this in the line sections shown in Fig. 3, where regions in between prevalent edges are significantly different between image J and the original image I. This is also observed by the larger MSE values reported, being higher for J than I^F. Solving the Poisson equation therefore has a non-local smoothing effect, while prevalent object edges act as the primal sketch and anchor the image during its reconstruction from the filtered gradient field.

We see that the image is smoothed by two processes, namely the RBAF anisotropic diffusion of the image gradient field and the least-squares method to reconstruct the image. While the roles they play in the four-step method are qualitatively understood, it is not possible to quantify their combined contribution a priori. Additionally, we note that the RBAF method is well suited for the image filtering due to the high accuracy of pseudo-spectral approximations to derivatives, and the robustness achieved by the fractional derivatives used in the regularisation process. Furthermore, fractional derivatives are non-local operators, providing function regularity, and have also been adopted for edge detection methods [37].

An automatic method for parameter selection (coefficient β and diffusion integration time T) has been used to ensure robustness and repeatability of the filtering process [27]. While the use of RBAF on the image or the image gradient field results in effectively two different orders of filtering, by standardising and automating the filtering process, we remove possible user bias and allow for repeatability of results. This consequently allows for a meaningful comparison between two-step and four-step methods, though one can foresee that superior results could potentially be obtained by adopting alternative automatic processes for each method. To also allow for meaningful comparison of results, the segmentation is performed using standard tools, namely the watershed method [4, 45] and the zero-crossing of the second directional derivatives [36, 11].

Finally we remark on the discrete difference schemes employed in both computing the image gradient field and in solving the Poisson equation. The finite difference stencils adopted are of low polynomial order and small stencil size, and are widely used. The frequency response of these digital differentiators is that of low-pass filters [49], which is well suited to the filtering procedures investigated here. In other applications these schemes may lead

to accentuated smoothness in the four-step process proposed, and higher order schemes may provide better results. It should be noted however that significant changes are not expected by adopting higher order schemes, since usually features of interest are described by discontinuities in the image, such as object edges. However, classical finite difference schemes (which are based on a polynomial fit) require regularity, and will thus always appear as under-resolved. Adopting methods such as essentially non-oscillatory (ENO), fractional derivatives or rational functions to derive discrete difference schemes, may have greater influence in the four-step procedure proposed.

Together, the results indicate an evident advantage in filtering the image gradient field instead of the image intensity directly. In practice, filtering the image gradient field has the advantage of reducing the noise more effectively, while preserving the main features of the image. The image gradient provides a natural setting for highlighting key information in the image, such as the delineation of object and features. In this work we have implicitly assumed that the meaningful information is present in the image as objects with distinct regions, hence we are looking for features with the strongest gradients. The result of filtering the gradient field is effectively that of reducing noise and small gradient detail in the image, while preserving the dominant features. Having filtered the gradient field to retain the dominant gradient features, these act as the skeletal frame from which the image is then reconstructed with the least-squares approach.

5. Conclusions

A four-step method is proposed for gradient-based filtering and object segmentation in medical images. These steps are: i) compute the image gradient field using a low-pass finite different scheme; ii) filter the components of the gradient field using the *regularised backward and forward anisotropic diffusion* (RBAF) method with appropriate parameter selection; iii) reconstruct the image from the modified gradient by solving a least-squares fit problem (hence solving for a Poisson equation); iv) perform the desired image segmentation. The parameters required in the RBAF model are set through an automatic procedure to allow for repeatability and robustness of the method.

Numerical tests on two-dimensional grey-scale images indicate that image gradient-based filtering outperforms the traditional image-based filtering with overall encouraging results. Results from the mammography image dataset showed accurate delineation of lesion tissue while reducing effects of over segmentation. Results from the confocal microscopy image dataset reported smooth edge detection of the red blood cells with accurate localisation and effective reduction of the background noise. The proposed four-step method implicitly assumes that the objects of interest are evident, such that the image gradient magnitude provides clear information regarding these object edges. Consequently the non-linear anisotropic filtering will not remove these edges, but rather will act to further highlight them with respect to other less marked features in the image.

We observe that filtering noise in the image gradient field is effective, since noise is readily perceived. The anisotropic diffusion method allows for smoothing to occur within regions, resulting in smoother object edges and more uniform object contrast. Reconstructing the

final image from the modified gradient field is based on a least-squares fit, hence non-local smoothing will occur by solving the Poisson equation, which acts to further remove noise and improve contrast. Finally, the low-pass finite difference stencils used to compute the image gradient field as well as solve for the Poisson equation, also act to provide a smooth reconstructed final image.

Further developments of the proposed method could attempt combining the first three stages into a single higher-order PDE filtering scheme, similar to existing higher-order PDE-based filters. While this is appealing, since greater physical understanding can be obtained from a PDE model, it is not evident how to achieve the non-local smoothing provided currently by solving the least-squares problem to reconstruct the final image from a modified gradient field. The least-squares reconstruction acts to smooth the image based on the dominant image gradient information, and leads to clearer and more uniform contrast at boundary edges, improving the segmentation obtained, and is consequently an important step in the proposed method. Finally, the filtering of the image gradient field can easily be extended to three-dimensional image datasets, which may be appealing when volumetric image datasets are considered.

Acknowledgements

The authors gratefully acknowledge support from Fundação para a Ciência e a Tecnologia (FCT) through the grant SFRH/BD/52326/2013, in particular project 'Physiomath' (EXCL/MAT-NAN/0114/2012). The confocal microscopy data sets are gratefully provided by Prof. Rui Lima and his research team from Universidade do Minho, supported by FCT project 'Biomimetic' (BIOMIMETICPTDC/SAU-ENB/116929/2010).

References

[1] R. Anderssen and F. De Hoog. Finite difference methods for the numerical differentiation of non-exact data. *Computing*, 33(3-4):259–267, 1984.

[2] P. G. Barten. *Contrast sensitivity of the human eye and its effects on image quality*, volume 72. SPIE press, 1999.

[3] R. Bernardes, C. Maduro, P. Serranho, A. Araújo, S. Barbeiro, and J. Cunha-Vaz. Improved adaptive complex diffusion despeckling filter. *Optics express*, 18(23):24048–24059, 2010.

[4] S. Beucher. The watershed transformation applied to image segmentation. *SCANNING MICROSCOPY-SUPPLEMENT-*, pages 299–299, 1992.

[5] J. Cullum. Numerical differentiation and regularization. *SIAM Journal on numerical analysis*, 8(2):254–265, 1971.

[6] R. Fattal, D. Lischinski, and M. Werman. Gradient domain high dynamic range compression. In *ACM transactions on graphics (TOG)*, volume 21, pages 249–256. ACM, 2002.

[7] D. J. Field, A. Hayes, and R. F. Hess. Contour integration by the human visual system: evidence for a local association field. *Vision research*, 33(2):173–193, 1993.

[8] G. D. Finlayson, S. D. Hordley, and M. S. Drew. Removing shadows from images. In *European conference on computer vision*, pages 823–836. Springer, 2002.

[9] B. Fornberg and N. Flyer. Accuracy of radial basis function interpolation and derivative approximations on 1-d infinite grids. *Advances in Computational Mathematics*, 23(1-2):5–20, 2005.

[10] R. T. Frankot and R. Chellappa. A method for enforcing integrability in shape from shading algorithms. *IEEE Transactions on pattern analysis and machine intelligence*, 10(4):439–451, 1988.

[11] A. Gambaruto. Processing the image gradient field using a topographic primal sketch approach. *International journal for numerical methods in biomedical engineering*, 31(3), 2015.

[12] A. S. Georghiades, P. N. Belhumeur, and D. J. Kriegman. From few to many: Illumination cone models for face recognition under variable lighting and pose. *IEEE transactions on pattern analysis and machine intelligence*, 23(6):643–660, 2001.

[13] G. Gilboa, N. Sochen, and Y. Zeevi. Image enhancement and denoising by complex diffusion processes. *IEEE Transactions on Pattern Analysis and Machine Intelligence*, 26(8):1020–1036, 2004.

[14] J. Guidotti, Y. Kim, and J. Lambers. Image restoration with a new class of forward-backward-forward diffusion equations of perona–malik type with applications to satellite image enhancement. *SIAM Journal on Imaging Sciences*, 6(3):1416–1444, 2013.

[15] P. Guidotti. A new nonlocal nonlinear diffusion of image processing. *Journal of Differential Equations*, 246(12):4731–4742, 2009.

[16] P. Guidotti. A backward–forward regularization of the perona–malik equation. *Journal of Differential Equations*, 252(4):3226–3244, 2012.

[17] P. Guidotti. A family of nonlinear diffusions connecting perona-malik to standard diffusion. *Discrete Contin Dyn Syst Ser S*, 5(3):581–590, 2012.

[18] P. Guidotti and J. Lambers. Two new nonlinear nonlocal diffusions for noise reduction. *Journal of Mathematical Imaging and Vision*, 33(1):25–37, 2009.

[19] P. Guidotti and K. Longo. Two enhanced fourth order diffusion models for image denoising. *Journal of Mathematical Imaging and Vision*, 40(2):188–198, 2011.

[20] R. Haralick, L. Watson, and T. Laffey. The topographic primal sketch. *The International Journal of Robotics Research*, 2(1):50–72, 1983.

[21] M. Harker and P. O'Leary. Least squares surface reconstruction from measured gradient fields. In *Computer Vision and Pattern Recognition, 2008. CVPR 2008. IEEE Conference on*, pages 1–7. IEEE, 2008.

[22] M. Harker and P. OLeary. Regularized reconstruction of a surface from its measured gradient field. *Journal of Mathematical Imaging and Vision*, 51(1):46–70, 2015.

[23] B. K. Horn and M. J. Brooks. The variational approach to shape from shading. *Computer Vision, Graphics, and Image Processing*, 33(2):174–208, 1986.

[24] T. Huang, G. Yang, and G. Tang. A fast two-dimensional median filtering algorithm. *IEEE Transactions on Acoustics, Speech, and Signal Processing*, 27(1):13–18, 1979.

[25] Y.-L. Huang and D.-R. Chen. Watershed segmentation for breast tumor in 2-d sonography. *Ultrasound in medicine & biology*, 30(5):625–632, 2004.

[26] F. Jin, P. Fieguth, L. Winger, and E. Jernigan. Adaptive wiener filtering of noisy images and image sequences. In *Image Processing, 2003. ICIP 2003. Proceedings. 2003 International Conference on*, volume 3, pages III–349. IEEE, 2003.

[27] A. João, A. Gambaruto, R. Pereira, and A. Sequeira. Robust and effective automatic parameter choice for medical image filtering. *Computer Methods in Biomechanics and Biomedical Engineering: Imaging & Visualization*, 8(2):152–168, 2020.

[28] W. C. Karl, Z. Liang, H. Pien, and T. J. Brady. Medical image processing, Mar. 30 2010. US Patent 7,689,017.

[29] T. M. Lehmann, C. Gonner, and K. Spitzer. Survey: Interpolation methods in medical image processing. *IEEE transactions on medical imaging*, 18(11):1049–1075, 1999.

[30] S. K. Lele. Compact finite difference schemes with spectral-like resolution. *Journal of computational physics*, 103(1):16–42, 1992.

[31] R. Lima, T. Ishikawa, Y. Imai, M. Takeda, S. Wada, and T. Yamaguchi. Measurement of individual red blood cell motions under high hematocrit conditions using a confocal micro-ptv system. *Annals of biomedical engineering*, 37(8):1546–1559, 2009.

[32] J. Liu, X. Liu, J. Chen, and J. Tang. Mass segmentation in mammograms based on improved level set and watershed algorithm. In *International Conference on Intelligent Computing*, pages 502–508. Springer, 2011.

[33] J. Lovoie, T. J. Osler, and R. Tremblay. Fractional derivatives and special functions. *SIAM review*, 18(2):240–268, 1976.

[34] Z.-L. Lu and G. Sperling. The functional architecture of human visual motion perception. *Vision research*, 35(19):2697–2722, 1995.

[35] Z. Ma, J. M. R. Tavares, R. N. Jorge, and T. Mascarenhas. A review of algorithms for medical image segmentation and their applications to the female pelvic cavity. *Computer Methods in Biomechanics and Biomedical Engineering*, 13(2):235–246, 2010.

[36] D. Marr and E. Hildreth. Theory of edge detection. *Proceedings of the Royal Society of London B: Biological Sciences*, 207(1167):187–217, 1980.

[37] B. Mathieu, P. Melchior, A. Oustaloup, and C. Ceyral. Fractional differentiation for edge detection. *Signal Processing*, 83(11):2421–2432, 2003.

[38] P. Meer and I. Weiss. Smoothed differentiation filters for images. In *Pattern Recognition, 1990. Proceedings., 10th International Conference on*, volume 2, pages 121–126. IEEE, 1990.

[39] H.-S. Ng, T.-P. Wu, and C.-K. Tang. Surface-from-gradients without discrete integrability enforcement: a gaussian kernel approach. *IEEE Transactions on pattern analysis and machine intelligence*, 32(11):2085–2099, 2010.

[40] F. P. Oliveira and J. R. Tavares. Medical image registration: a review. *Computer methods in biomechanics and biomedical engineering*, 17(2):73–93, 2014.

[41] C. Pei, C. Wang, and S. Xu. Segmentation of the breast region in mammograms using marker-controlled watershed transform. In *The 2nd International Conference on Information Science and Engineering*, pages 2371–2374. IEEE, 2010.

[42] P. Perona and J. Malik. Scale-space and edge detection using anisotropic diffusion. *IEEE Transactions on pattern analysis and machine intelligence*, 12(7):629–639, 1990.

[43] L. I. Rudin, S. Osher, and E. Fatemi. Nonlinear total variation based noise removal algorithms. *Physica D: nonlinear phenomena*, 60(1-4):259–268, 1992.

[44] L. Shafarenko, M. Petrou, and J. Kittler. Automatic watershed segmentation of randomly textured color images. *IEEE transactions on Image Processing*, 6(11):1530–1544, 1997.

[45] P. Soille. Morphological carving. *Pattern Recognition Letters*, 25(5):543–550, 2004.

[46] G. Strang. The discrete cosine transform. *SIAM review*, 41(1):135–147, 1999.

[47] J. Suckling, J. Parker, D. Dance, S. Astley, I. Hutt, C. Boggis, I. Ricketts, E. Stamatakis, N. Cerneaz, S. Kok, et al. The mammographic image analysis society digital mammogram database. In *Exerpta Medica. International Congress Series*, volume 1069, pages 375–378, 1994.

[48] D. Van De Ville, M. Nachtegael, D. Van der Weken, E. E. Kerre, W. Philips, and I. Lemahieu. Noise reduction by fuzzy image filtering. *IEEE Transactions on fuzzy systems*, 11(4):429–436, 2003.

[49] R. Vichnevetsky and J. B. Bowles. *Fourier analysis of numerical approximations of hyperbolic equations*, volume 5. Siam, 1982.

[50] H. Wang, Y. Chen, T. Fang, J. Tyan, and N. Ahuja. Gradient adaptive image restoration and enhancement. In *2006 International Conference on Image Processing*, pages 2893–2896. IEEE, 2006.

[51] I. Weiss. High-order differentiation filters that work. *IEEE Transactions on Pattern Analysis and Machine Intelligence*, 16(7):734–739, 1994.

[52] N. Wiener. *Extrapolation, interpolation, and smoothing of stationary time series*, volume 2. MIT press Cambridge, 1949.

[53] G. A. Wood. Data smoothing and differentiation procedures in biomechanics. *Exercise and sport sciences reviews*, 10(1):308–362, 1982.

[54] S. Xu, H. Liu, and E. Song. Marker-controlled watershed for lesion segmentation in mammograms. *Journal of digital imaging*, 24(5):754–763, 2011.

[55] R. Zhang, P.-S. Tsai, J. Cryer, and M. Shah. Shape-from-shading: a survey. *IEEE transactions on pattern analysis and machine intelligence*, 21(8):690–706, 1999.